

Micro-swimmer collective dynamics in Brinkman flows

Yasser Almoteri^{1,2}, Enkeleida Lushi^{1*}

¹ *Mathematical Sciences, New Jersey Institute of Technology, Newark, NJ, 07102, United States*

² *Department of Mathematics and Statistics, Imam Mohammad Ibn Saud Islamic University, Riyadh 11623, Saudi Arabia*

(Dated: April 30, 2024)

Suspensions of swimming micro-organisms are known to undergo intricate collective dynamics as a result of hydrodynamic and collision interactions. Micro-swimmers, such as bacteria and microalgae, naturally live and have evolved in complex habitats that include impurities, obstacles and interfaces. To elucidate their dynamics in a heterogeneous environment, we consider a continuum theory where the micro-swimmers are embedded in a Brinkman wet porous medium, which models viscous flow with an additional resistance or friction due to the presence of smaller stationary obstacles. The conservation equation for the swimmer configurations includes advection and rotation by the immersing fluid, and is coupled to the viscous Brinkman fluid flow with an active stress due to the swimmers' motion in it. Resistance alters individual swimmer locomotion and the way it disturbs the surrounding fluid, and thus it alters its hydrodynamic interactions with others and such affects collective dynamics. The entropy analysis and the linear stability analysis of the system of equations both reveal that resistance delays and hinders the onset and development of the collective swimming instabilities, and can completely suppress it if sufficiently large. Simulations of the full nonlinear system confirm these. We contrast the results with previous theoretical studies on micro-swimmers in homogeneous viscous flow, and discuss relevant experimental realizations.

I. INTRODUCTION

Micro-organisms are naturally found in many diverse environments, from phytoplankton in the oceans, to microbes in soil and volcanic hot springs, to microbes in plants and animals's bodies [1–9]. Micro-swimmers such as bacteria are important in nutrient recycling, digestion, fermentation, bioremediation, nitrogen fixation from the atmosphere, and some pathogenic ones can cause infectious diseases. Micro-swimmers such as algae are utilized in photo-bioreactors and drug production. Micro-swimmers such as spermatozoa are crucial in the propagation of many species of animals. Additionally, artificial active particles such as phoretic colloids or driven colloids [10–13] have been inspired by natural micro-swimmers. Given their ubiquity and importance in nature and technology, studying micro-swimmers' behavior, motion, collective dynamics, interactions with the environment, and their response to nutrients or toxins, is paramount to understanding many phenomena they are involved in.

Many experiments studied how microorganisms or other “active” particles affect the fluid they live in, how they interact with each-other through it, and how hydrodynamic and collision interactions affect the emerging collective motion [14–22]. Macroscopic patterns are known to emerge as a result of hydrodynamic interactions and collisions between the micro-swimmers, and they depend on the swimmer type and geometry [6, 23–28]. Significant work has been done on the micro-swimmer collective dynamics emerging due to hydrodynamic or chemotactic interactions not both, e.g. using continuum models [24, 29–50] or direct simulations [23, 26–28, 45, 51–66].

Although micro-swimmers naturally live and move in non-trivial environments and confinements such as tissues, soils and sediments, most experimental studies with microbes focus on homogeneous environments such as bulk liquid or flat surfaces [5, 7, 9, 67]. Experimental studies have been conducted on micro-swimmers in complex confinement, for example the colony stability and organization in large drops, racetracks or pillar forests [27, 28, 68–74], the motion or transport of swimmers in disordered media with quasi-2D obstacles [7, 73–79], or in 3D porous environments [80, 81]. Recent experiments have shown that 3D pore-scale confinement strongly affects micro-swimmer locomotion and migration [80–82] and it alters the dynamics and morphology of the migrating bacterial population [76, 83–86]. Theoretical and computational studies of bacterial chemotactic motion in wet porous environments catching up, for example recent work has incorporated the porosity effects by modifying the standard motility parameters substantially from their bulk liquid values [83, 87].

The difficulty with theoretical and computational modeling of active matter in such complex confinements rests with the impossible task of properly and resolving the hydrodynamical interactions as well collisions with the swimmers with each-other and any non-trivially-shaped surface or obstacle in their surrounding. Continuum models are more appropriate to model population dynamics, however one cannot faithfully include the effects of the swimmer collisions, which are crucial in determining the confined dynamics [27, 28, 70, 71] and can at most approximate them [39]. Numerical simulations of the coupled dynamics of individually-traced micro-swimmers on the other hand are often not feasible for realistic numbers of swimmers because the difficulty and computational cost involved in resolving the non-local interactions such as hydrodynamical ones. Approximations

* YKAlmoteri@imamu.edu.sa; lushi@njit.edu

can be made in special cases, e.g. individual swimmers in viscoelastic or power-law flows [88–90], or collective behavior in complex or viscoelastic flows when the intra-swimmer and swimmer-boundary interactions may not be directly included [67, 91–97]. An extra special case however is Brinkman flow, which due to its linearity has made possible studies of individual squirmer dynamics or flagellar swimmers moving through it [98–103].

Despite the relative simplicity of the Brinkman fluid flows, there have not yet been any studies of micro-swimmer collective dynamics in them, which is the question that we will address in this paper. We will present a continuum model, building on many well-known coarse-grained models mentioned before [24, 25, 29–46, 48–50] where we couple the micro-swimmer dynamics to that of the Brinkman viscous flow that they are immersed in.

In the present work we describe a simple continuum model, derived from first principles, to study the dynamics of dilute micro-swimmer suspensions that are immersed in a viscous Brinkman fluid. The model consists of a conservation equation for the swimmer configuration distributions, which is based on the equations for the motion of a self-propelling rod in a local linear flow, and it is coupled to the Brinkman equation for the fluid motion with an extra stress due to the forcing exerted by the swimmers in it. We analyze the configurational entropy and the stability of the linearized system of uniform isotropic suspensions, and show that the Brinkman resistance hinders the emergence of the long-wave instabilities predicted and well-studied for Stokesian suspensions [24, 104]. We perform simulations of the full nonlinear system where the predictions of the linear analysis are confirmed, and investigate the long-time evolution of the instabilities and the pattern formation. The analysis and simulations all show that the Brinkman resistance term hinders the onset and development of the collective swimming instabilities.

II. SWIMMING IN BRINKMAN FLOW

Microorganisms often encounter viscous environments that are heterogeneous and contain stationary obstacles or inert impurities immersed within the fluid medium. Examples are bacteria living in soil [105], pathogens like bacteria or certain spirochetes navigating heterogeneous tissues in the body [81, 106]. In such scenarios, to depict the flow of a viscous fluid through spherical particles that are smaller than the flow’s characteristic length scale [107], one can utilize the *Brinkman approximation* [108–110], which can be viewed as the incorporation of a lower-order resistance term into the Stokes equations for viscous flow [100, 101].

A. Brinkman flow and its disturbances

The Brinkman Equations to describe viscous flow in a such porous medium are:

$$\mu \nabla^2 \mathbf{u} - \nabla p - \frac{\mu}{K_D} \mathbf{u} = 0, \quad \nabla \cdot \mathbf{u} = 0 \quad (1)$$

where μ is the viscosity, \mathbf{u} is the fluid velocity, p is the fluid pressure, and $K_D > 0$ is the constant Darcy permeability. After non-dimensionalization with a lengthscale L , velocity-scale U , $\frac{\mu U}{L}$ the pressure scale, we obtain

$$\nabla^2 \mathbf{u} - \nabla p - \nu^2 \mathbf{u} = 0, \quad \nabla \cdot \mathbf{u} = 0 \quad (2)$$

where $\nu = \frac{L}{\sqrt{k}}$ is the ratio of the particle dimension to the permeability length of the medium [107]. We will refer to ν as the resistance parameter.

The Green’s function for the Brinkman Equations, commonly referred to as the *Brinkmanlet* [107] is:

$$\mathbf{B}(\mathbf{r}) = H_1(r)\mathbf{I} + H_2(r)\mathbf{r}\mathbf{r}^T \quad (3)$$

with \mathbf{I} the identity matrix, $r = |\mathbf{x} - \mathbf{x}_0|$ and

$$H_1(r) = \frac{e^{-\nu r}}{4\pi r} \left(\frac{1}{\nu^2 r^2} + \frac{1}{\nu r} + 1 \right) - \frac{1}{4\pi \nu^2 r^3},$$

$$H_2(r) = -\frac{e^{-\nu r}}{4\pi r^3} \left(\frac{3}{\nu^2 r^2} + \frac{3}{\nu r} + 1 \right) + \frac{3}{4\pi \nu^2 r^5}.$$

The fluid flow velocity due to a force \mathbf{f} applied in a Brinkman fluid is then computed by $\mathbf{u}(\mathbf{x}) = \mathbf{B}(\mathbf{r})\mathbf{f}$.

The Brinkmanlet formula can be used in free-space domains, though modifications can be sometimes achieved for half-space domains [101, 111]. A regularized Brinkmanlet solution can be derived for a “blob” or regularized force [98, 107]. In periodic domains it is possible to solve the Brinkman Equations with a more general force [112], as we will also show and use later.

When a point force is applied to a viscous fluid or Stokes flow, the velocity disturbance that follows it decays as $1/r$ with distance r , as seen in Fig. 1. However in a Brinkman medium the decay of the velocity disturbance is significantly altered at large distances and decays much faster, at a rate of $1/r^3$ [110] because a new length-scale has been introduced into the problem. These effects are illustrated in Fig. 1: the disturbance fluid flow is not as long-ranged as in the Stokes case.

In Fig. 2 we plot the fluid flow generated by a force dipole (two opposite direction forces applied at a small offset distance) in Brinkman flow of various resistance values. The fluid flow generated by this force dipole, illustrating the highest order of the disturbance fluid flow generated by a micro-swimmer moving through it, is also visibly affected by the medium resistance. Notably, the fluid flow becomes more localized and its effects are not felt as far as in a pure viscous flows.

Figures 1 and 2 illustrate the motivation of our study.

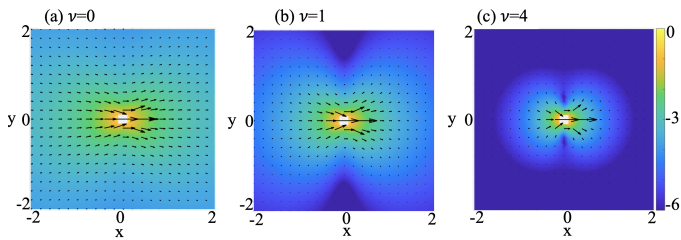


FIG. 1. Fluid velocity generated when the force $\mathbf{f} = (1, 0, 0)$ is applied at point $\mathbf{x}_0 = (0, 0, 0)$ in a Brinkman flow with different hydrodynamic resistances: $\nu = 0, 1, 4$. The vector field indicates \mathbf{u} , whereas the field color represents $\log|\mathbf{u}|$.

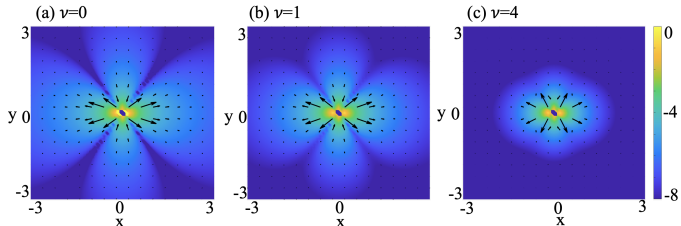


FIG. 2. Fluid velocity generated by two closely-applied opposite forces in Brinkman flow with different hydrodynamic resistances: $\nu = 0, 1, 4$. The vector field indicates \mathbf{u} , whereas the field color represents $\log|\mathbf{u}|$.

Given that resistance alters the fluid flow disturbance generated by a swimmer moves through a Brinkman fluid [99–103, 112], and given that locomotion-generated fluid disturbances and overall hydrodynamic interactions affect the emergence of macroscopic collective behavior in micro-swimmer suspensions [6, 23, 24, 32, 33, 35, 38, 42, 43, 45, 46, 48, 104], how is the collective motion in Brinkman suspensions affected?

B. Propulsive rod in Brinkman flow

We outline the derivation of the equations of motion for a slender rigid swimmer embedded in a Brinkman flow, adapting from similar derivations for slender swimmers in Stokes flow [23, 113]. Let the swimmer with length ℓ have centerline $\mathbf{X}(s, t) = \mathbf{X}_c(t) + s\mathbf{p}(t)$, where s is its arclength, $-\ell/2 \leq s \leq \ell/2$, \mathbf{X}_c its center of mass, \mathbf{p} its orientation ($|\mathbf{p}| = 1$), and let the centerline's velocity be $\mathbf{V}(s, t)$. The local slender-body approximation [23, 113–116] says

$$\eta[\mathbf{V}(s, t) - \mathbf{u}(\mathbf{X}, t)] = (\mathbf{I} + \mathbf{X}_s \mathbf{X}_s^T) \mathbf{f}, \quad (4)$$

where $\mathbf{u}(\mathbf{X}, t)$ the linearized local background fluid flow around the swimmer's body, \mathbf{f} the force per unit length exerted by the swimmer upon the fluid, $\eta = 8\pi\mu/|\ln(\epsilon\epsilon^2)|$ with $\epsilon \ll 1$ the swimmer aspect ratio.

Following Hohenegger and Shelley [113], we consider the swimmer's propulsive stress to be applied tangentially to the lower half of its length, and a no-slip

condition applied to the front half. The model represents a *pusher* micro-swimmer for which the thrust is generated at the rear, akin to motile bacteria and spermatozoa. On the flower half ($s < 0$), the constant propulsive tangential stress $\mathbf{f}_1 = -f_{\parallel}\mathbf{p} = -(f_0 + f_1)s\mathbf{p}$ with $f_0 = 2\pi ag$ is posed, where a here is the swimmer radius and g the stress magnitude. A surface slip velocity is imposed $\mathbf{u}_s = u_s(s)\mathbf{p}$. Eq. (4) becomes

$$\begin{aligned} \eta[\dot{\mathbf{X}}_c + u_s\mathbf{p} + s\dot{\mathbf{p}} - \nabla\mathbf{u}] &= (\mathbf{I} + \mathbf{X}_s \mathbf{X}_s^T) \mathbf{f}_1, s < 0 \\ \eta[\dot{\mathbf{X}}_c + s\dot{\mathbf{p}} - \nabla\mathbf{u}] &= (\mathbf{I} + \mathbf{X}_s \mathbf{X}_s^T) \mathbf{f}_2, s > 0 \end{aligned} \quad (5)$$

Using the zero force and zero torque conditions on the swimmer upon integrating Eq. 5 in arclength, and the fact that \mathbf{f} is parallel to \mathbf{p} and, we can solve for the force \mathbf{f} per unit length exerted by the rod on the fluid:

$$\begin{aligned} \mathbf{f} = \mathbf{f}_1 &= -f_0\mathbf{p} - (\eta/2)\mathbf{p}^T \nabla\mathbf{u}\mathbf{p}\mathbf{p}, \quad -\ell/2 \leq s < 0 \\ \mathbf{f} = \mathbf{f}_2 &= f_0\mathbf{p} - (\eta/2)\mathbf{p}^T \nabla\mathbf{u}\mathbf{p}\mathbf{p}, \quad 0 \leq s \leq \ell/2, \end{aligned} \quad (6)$$

and the kinematic equations for the swimming rod:

$$\dot{\mathbf{X}}_c = \mathbf{u} + U\mathbf{p}. \quad (7)$$

$$\dot{\mathbf{p}} = (\mathbf{I} - \mathbf{p}\mathbf{p}^T)\nabla\mathbf{u}\mathbf{p}. \quad (8)$$

We have let $U := -u_s/2 = \epsilon|\ln(\epsilon\epsilon^2)|\ell g/\mu$ be the swimming speed of a single propulsive rod of length ℓ .

C. Extra active stress

Kirkwood's and Batchelor's formulas for the extra-stress produced by slender bodies suspended in Newtonian flows [117–120] lead to

$$\Sigma^{(p)} = -\frac{1}{V} \sum_{m=1}^N \int_{\partial B_m} ds \mathbf{f} \mathbf{X}^T \quad (9)$$

for the microscopic stress $\Sigma^{(p)}$ evaluated on the surfaces ∂B_m of N slender swimmer bodies in a volume V [113]. Using Eq. (6), the contribution to the stress from one swimmer is

$$\mathbf{S}^p = -f_0\ell^2/2\mathbf{p}\mathbf{p}^T = -\sigma_0\mathbf{p}\mathbf{p}^T, \quad (10)$$

where the units of $\sigma_0 = \pi\epsilon\ell^3g$ are force times length: the units of the strength of a stresslet or force dipole.

Combining Eqs. (9) and (10), we find the volume-averaged extra stress in a box of volume L^3 containing N swimmers. We assume there are M swimmers in a smaller control volume L_M^3 and that the rate-of-strain tensor is constant over this smaller volume. Furthermore, we suppose a separation of scales ($\ell \leq L_M \leq L$). We find

$$\Sigma^{(p)} = -n\Phi\sigma_0 \frac{1}{M} \sum_{m=1}^M \mathbf{p}\mathbf{p}^T, \quad (11)$$

where $n = N/L^3$ is the number density and $\Phi = (M/L_M^3)/(N/L^3)$ is the local swimmer concentration.

As explained by [113], for large M , the weighted sum converges to the configurational average with respect to Ψ_M , the probability density function for finding a propulsive rod with a given center-of-mass position and orientation in the small volume. Going from the local distribution function and concentration to the macroscopic distribution function, we write $\Psi_M = \Psi/\Phi$ and the extra stress becomes $\Sigma(\mathbf{p}) = -n\sigma_0 \langle \mathbf{p}\mathbf{p}^T \rangle$. Redefining Ψ as $n\Psi$, we obtain the extra stress generated by a suspension of rear-activated rode-like swimmers

$$\Sigma^p(\mathbf{x}, t) = -\sigma_0 \langle \mathbf{p}\mathbf{p}^T \rangle = -\sigma_0 \int d\mathbf{p} \Psi \mathbf{p}\mathbf{p}^T. \quad (12)$$

Lastly, and also following [113], we coarse-grain the kinematic equations of motions for an ensemble of slender swimmers:

$$\dot{\mathbf{x}} = U\mathbf{p} + \mathbf{u} - D\nabla_x(\ln \Psi) \quad (13)$$

$$\dot{\mathbf{p}} = (\mathbf{I} - \mathbf{p}\mathbf{p}^T)\nabla\mathbf{u} - d_r\nabla_{\mathbf{p}}(\ln \Psi), \quad (14)$$

where we introduced translational and rotational diffusion with phase-space (not particle) coefficients D and d_r [23, 24, 113, 119]. Eqs. (13) are particles translational and rotational fluxes [24, 25, 33, 113].

Eqs. (7, 12) lie at the heart of many continuum descriptions of active suspensions in Stokes flow [6]. It is worth mentioning that the equations of motion for the swimmer Eq. (7), the particle fluxes Eq. (13) and the extra stress Eqs. (12) are identical to the case of the Stokes flow because Brinkman flow is linear. The difference between will lie solely in the presence of the resistance term in the Brinkman equations.

III. MATHEMATICAL MODEL

A. Continuum theory of micro-swimmers in Brinkman flow

The probability distribution function $\Psi(\mathbf{x}, \mathbf{p}, t)$ represents the configuration of ellipsoidal micro-swimmers, where \mathbf{x} denotes the swimmer center of mass and \mathbf{p} denotes the direction with ($|\mathbf{p}| = 1$). The dynamics of swimmers in such a suspension is described by a conservation equation that takes into account fluid advection and rotation as well as the diffusion of particles:

$$\begin{aligned} \frac{\partial \Psi}{\partial t} = & -\nabla_x \cdot [\Psi(U_0\mathbf{p} + \mathbf{u})] \\ & -\nabla_p \cdot [\Psi(\mathbf{I} - \mathbf{p}\mathbf{p}^T)(\gamma\mathbf{E} + \mathbf{W})\mathbf{p}] \\ & + D\nabla_x^2 \Psi + d_r\nabla_p^2 \Psi. \end{aligned} \quad (15)$$

Eq. (15) includes flux velocities in the center of mass

\mathbf{x} and orientation \mathbf{p} :

$$\dot{\mathbf{x}} = U_0\mathbf{p} + \mathbf{u} - D\nabla_x(\ln \Psi) \quad (16)$$

$$\dot{\mathbf{p}} = (\mathbf{I} - \mathbf{p}\mathbf{p}^T)[(\gamma\mathbf{E} + \mathbf{W})\mathbf{p}] - d_r\nabla_p(\ln \Psi), \quad (17)$$

as also derived in Eq. (7) in the case of slender swimmers. The translational velocity in Eq. (16) is the sum of the background fluid velocity \mathbf{u} and propulsion with constant swimming speed U_0 along orientation \mathbf{p} . We model isotropic translational diffusion with a constant D . Here $\nabla_{\mathbf{p}}$ is the gradient operator on the sphere. Eq. (17) is Jeffery's equation [121] for the angular velocity in terms of the fluid rate-of-strain \mathbf{E} , vorticity tensor \mathbf{W} and a shape parameter $-1 \leq \gamma \leq 1$ (where $\gamma = 0$ for a sphere and $\gamma \approx 1$ for a rod). It captures the rotation of an anisotropic particle in the local flow. Angular diffusion is included with a constant rotational diffusion coefficient d_r [24, 46?].

Eq. (15) does not include a term for micro-swimmer run-and-tumble behavior, though basal tumbling with isotropic or anisotropic is possible to incorporate [6, 32, 35, 38, 43, 48, 122].

Microscopic organisms encounter varying fluid environments that contain networks of stationary obstacles suspended within them. The flow of viscous fluid through these porous materials can be modeled by adding an additional hydrodynamic resistance or friction term, $\frac{\mu}{K_D}\mathbf{u}$, to the Stokes-Brinkman equations. The Brinkman equation was developed to model the flow through a porous material containing scattered spherical particles [98, 110, 123].

When micro-swimmers are present, the fluid velocity $\mathbf{u}(\mathbf{x}, t)$ satisfies the Stokes-Brinkman equations with an extra active stress due to the swimmers' motion in it:

$$-\mu\nabla_x^2\mathbf{u} + \nabla_x q + \frac{\mu}{K_D}\mathbf{u} = \nabla_x \cdot \Sigma^p, \quad (18)$$

$$\nabla_x \cdot \mathbf{u} = 0. \quad (19)$$

Here μ is the viscosity, q the fluid pressure, $K_D > 0$ the constant Darcy permeability, and Σ^p is the active stress, as also derived in Eq. (12) in the case of slender swimmers:

$$\Sigma^p(\mathbf{x}, t) = \sigma_0 \int \Psi(\mathbf{x}, \mathbf{p}, t)(\mathbf{p}\mathbf{p}^T - \mathbf{I}/3)d\mathbf{p}. \quad (20)$$

The active stress Σ^p is the average configuration of the active stresses $\sigma_0(\mathbf{p}\mathbf{p}^T - \mathbf{I}/3)$ that are exerted on the fluid by the swimmers over all possible orientations \mathbf{p} [25, 117, 124?]. Lastly, $\sigma_0 = U_0\mu\ell^2\alpha$, where ℓ is the characteristic swimmer length and α is an $O(1)$ dimensionless constant whose value depends on the mechanism of swimming and swimmer geometry. Swimmers with rear-activated propulsion, like motile bacteria *E. coli* or spermatozoa, are called pushers, and have a negative stresslet strength $\sigma_0 < 0$ and a negative value for α . Swimmers with front-propulsion, like *C. reinhardtii*, are called pullers, and have $\sigma_0 > 0$ and $\alpha > 0$ [24, 46?].

We define the local swimmer concentration $\Phi(\mathbf{x}, t)$ and the mean swimmer director $\langle \mathbf{p}(\mathbf{x}, t) \rangle$ as

$$\Phi(\mathbf{x}, t) = \int d\mathbf{p} \Psi(\mathbf{x}, \mathbf{p}, t), \quad (21)$$

$$\langle \mathbf{p}(\mathbf{x}, t) \rangle = \int d\mathbf{p} \mathbf{p} \Psi(\mathbf{x}, \mathbf{p}, t). \quad (22)$$

B. Non-dimensionalization of the system

We non-dimensionalize Eq. (15) using the distribution, velocity, length and time scales $\Psi_c = n$, $u_c = U_0$, $l_c = (nl^2)^{-1}$, $t_c = l_c/u_c$, with $l_c = (V/V_p)l$ and $V_p = Nl^3$ the effective volume taken by N swimming particles of length l in the fluid volume V of a cube with length L [24]. n is the mean number density of the micro-swimmers in the volume V . This choice of non-dimensionalization normalizes the distribution function $(1/V) \int_V d\mathbf{x} \int d\mathbf{p} \Psi(\mathbf{x}, \mathbf{p}, t) = 1$ with $\Psi_0 = 1/4\pi$ the probability density for the uniform isotropic state.

We also non-dimensionalize the diffusions as $D' = Dt_c/l_c^2$, $d'_r = d_r t_c$. Dropping the '-s, the non-dimensionalized swimmer distribution equation becomes:

$$\frac{\partial \Psi}{\partial t} = -\nabla_x \cdot [\Psi(\mathbf{p} + \mathbf{u})] - \nabla_p \cdot [\Psi(\mathbf{I} - \mathbf{p}\mathbf{p}^T)(\gamma\mathbf{E} + \mathbf{W})\mathbf{p}] + D\nabla_x^2 \Psi + d_r \nabla_p^2 \Psi. \quad (23)$$

The fluid equations are non-dimensionalized using $\alpha = \sigma_0/(U_0\mu l_c^2)$ for α a non-dimensional $O(1)$ constant whose sign tells whether the micro-swimmers are pushers ($\alpha < 0$), pullers ($\alpha > 0$) [24, 46]. The non-dimensional permeability parameter is $\nu = l_c/\sqrt{K_D}$, and we will refer to it as the hydrodynamic resistance. The non-dimensional Stokes-Brinkman fluid equations are:

$$-\nabla_x^2 \mathbf{u} + \nabla_x q + \nu^2 \mathbf{u} = \nabla_x \cdot \Sigma^p, \quad \nabla_x \cdot \mathbf{u} = 0$$

$$\Sigma^p = \alpha \int \Psi(\mathbf{x}, \mathbf{p}, t) [\mathbf{p}\mathbf{p}^T - \mathbf{I}/3] d\mathbf{p}. \quad (24)$$

We make a note on the unusual non-dimensionalization choice for the characteristic lengthscale $l_c = (V/V_p)l = 1/(nl^2)$, which largely follows previous work on this topic [24, 25, 38, 39, 46]. See that $\alpha = (\sigma_0/\mu U_0 l^2)N(l/L)^3$ and $\nu = (1/K_D)N(l/L)^3$, so the number of swimmers N and hence their mean number density n is encapsulated into the strength of the swimmer effect into the fluid, α , and well as the strength of the resistance, ν .

C. The system in two dimensions

Since the numerical simulations presented later are in 2D, we briefly discuss the equations. In 2D, we have only one orientation angle, $\theta \in [0, 2\pi]$ with $\mathbf{p} = (\cos\theta, \sin\theta)$. The 2D model does not differ much in appearance from the 3D one in Eq. (15) except that in 2D, we have the

isotropic state $\Psi_0 = 1/2\pi$.

$$\frac{\partial \Psi}{\partial t} = -\nabla_x \cdot [\Psi(\mathbf{p} + \mathbf{u})] - \partial_\theta [\Psi \mathbf{p}_\perp^T (\gamma\mathbf{E} + \mathbf{W})\mathbf{p}] + D\nabla_x^2 \Psi + d_r \nabla_\theta^2 \Psi. \quad (25)$$

where $\mathbf{p}_\perp = (-\sin\theta, \cos\theta)$ is the unit vector perpendicular to the particle orientation. These are coupled to the fluid equations with active particle stress and additional hydrodynamic resistance or friction in the Stokes-Brinkman equations,

$$-\nabla_x^2 \mathbf{u} + \nabla_x q + \nu^2 \mathbf{u} = \nabla_x \cdot \Sigma^p, \quad \nabla_x \cdot \mathbf{u} = 0$$

$$\Sigma^p = \alpha \int_0^{2\pi} \Psi(\mathbf{x}, \theta, t) (\mathbf{p}\mathbf{p} - \mathbf{I}/2) d\theta. \quad (26)$$

IV. CONFIGURATIONAL ENTROPY

As in Saintillan and Shelley [25, 33], we define the system's configurational entropy \mathcal{S} as

$$\mathcal{S} = \int d\mathbf{x} s = \int d\mathbf{x} \int d\mathbf{p} \frac{\Psi}{\Psi_0} \ln\left(\frac{\Psi}{\Psi_0}\right), \quad (27)$$

with $\Psi_0 = 1/4\pi$ and $s = \int d\mathbf{p} (\Psi/\Psi_0) \ln(\Psi/\Psi_0)$. Note that $\mathcal{S} = \int d\mathbf{x} s(\mathbf{x}, t) \geq 0$ and \mathcal{S} realizes its minimum value of zero only for $\Psi = \Psi_0$, the homogeneous and isotropic state.

Differentiating s with respect to time and using the identity $\nabla_p \cdot [(\mathbf{I} - \mathbf{p}\mathbf{p}^T)\nabla_x \mathbf{u} \mathbf{p}] = -3\mathbf{p}\mathbf{p}^T : \mathbf{E}$, we obtain:

$$s_t + \mathbf{u} \cdot \nabla_x s + \nabla_x \cdot \int d\mathbf{p} (\Psi/\Psi_0) \ln(\Psi/\Psi_0) \mathbf{p}$$

$$= D\nabla_x^2 s + 3 \left(\int d\mathbf{p} (\Psi/\Psi_0) \mathbf{p}\mathbf{p}^T \right) : \mathbf{E}$$

$$- \int d\mathbf{p} [D|\nabla_x \ln(\Psi/\Psi_0)|^2 + d_r |\nabla_p \ln(\Psi/\Psi_0)|^2]. \quad (28)$$

The momentum equation in Eq. (24) can be integrated over the fluid domain to get:

$$2 \int d\mathbf{x} \mathbf{E} : \mathbf{E} + \nu^2 \int d\mathbf{x} |\mathbf{u}|^2 = - \int d\mathbf{x} \mathbf{E} : \Sigma^p. \quad (29)$$

Integrating Eq. (28) in \mathbf{x} and using the Eq. (29) gives, ultimately gives an *exact* equation for the evolution of the configurational entropy:

$$\Psi_0 \mathcal{D}_t \mathcal{S} = \frac{-6}{\alpha} \int d\mathbf{x} \mathbf{E} : \mathbf{E} - \nu^2 \int d\mathbf{x} |\mathbf{u}|^2$$

$$- \int d\mathbf{x} \int d\mathbf{p} \Psi [D|\nabla_x \ln \Psi|^2 + d_r |\nabla_p \ln \Psi|^2]. \quad (30)$$

In Eq. (30), we notice three distinctive contributions to the configurational entropy from the hydrodynamics, resistance, and diffusive processes.

The first term in the right hand side of Eq. (30) contains the rate of viscous dissipation $\int d\mathbf{x} \mathbf{E} : \mathbf{E}$ which is positive definite, hence, in the absence of any external forcing or boundaries, for suspensions of pullers ($\alpha > 0$) any fluctuations from the isotropic state as measured by the entropy are expected to monotonically dissipate, whereas for suspensions of pushers ($\alpha < 0$) there is a feedback loop where fluctuations create velocity gradients which further increase fluctuations [24, 25]. These are balanced by the diffusive processes in the system, seen in the third term in the right hand side of Eq. (30).

Last, but not least, the hydrodynamic resistance makes an appearance in the second term of Eq. (30). As $\int d\mathbf{x} |\mathbf{u}|^2$ is positive definite and $\nu^2 \geq 0$, it is clear that the resistance is expected to dampen any fluctuations from the isotropic state, thus having a stabilizing effect on the system. This expectation is supported by the results of our linear stability analysis of the isotropic state, as well as by the results of our nonlinear simulations, both presented in subsequent sections.

V. LINEAR STABILITY

A. The eigenvalue problem

We now consider the stability of a nearly uniform and isotropic swimmer suspension. For simplicity, we neglect angular diffusion $d_r = 0$ but we retain translational diffusion D . Let the swimmer suspension be a plane wave perturbation about the uniform isotropic state $\Psi = \Psi_0 = 1/4\pi$ and zero fluid flow $\mathbf{u}_0 = \mathbf{0}$ as:

$$\begin{aligned} \Psi(\mathbf{x}, \mathbf{p}, t) &= 1/4\pi + \epsilon \tilde{\Psi}(\mathbf{p}, \mathbf{k}) \exp(i\mathbf{k} \cdot \mathbf{x} + \sigma t) \\ \mathbf{u}(\mathbf{x}, \mathbf{p}, t) &= \mathbf{0} + \epsilon \tilde{\mathbf{u}}(\mathbf{p}, \mathbf{k}) \exp(i\mathbf{k} \cdot \mathbf{x} + \sigma t), \end{aligned}$$

with $|\epsilon| \ll 1$, \mathbf{k} the wavenumber, $\sigma(k)$ the growth rate.

Substituting these into the linearized system, we get an equation that is linear in $\tilde{\Psi}$:

$$(\sigma + i\mathbf{p} \cdot \mathbf{k} + Dk^2) \tilde{\Psi} = \frac{3}{2} i\gamma \Psi_0 \mathbf{p}^T (\hat{\mathbf{u}} \mathbf{k}^T + \mathbf{k} \hat{\mathbf{u}}^T) \mathbf{p}.$$

Letting $\mathbf{k} = k\hat{\mathbf{k}}$, we solve the fluid equations

$$\tilde{\mathbf{u}} = \frac{ik}{k^2 + \nu^2} (\mathbf{I} - \hat{\mathbf{k}} \hat{\mathbf{k}}^T) \tilde{\Sigma}^p \hat{\mathbf{k}}, \quad (31)$$

$$\tilde{\Sigma}^p = \alpha \int \tilde{\Psi}' \mathbf{p}' \mathbf{p}'^T d\mathbf{p}'. \quad (32)$$

Finally, plugging this into the $\tilde{\Psi}$ equation, we get

$$\begin{aligned} &(\sigma + i\mathbf{p} \cdot \mathbf{k} + Dk^2) \tilde{\Psi} \\ &= -\frac{3\gamma k^2}{4\pi(k^2 + \nu^2)} \mathbf{p}^T (\mathbf{I} - \hat{\mathbf{k}} \hat{\mathbf{k}}^T) \tilde{\Sigma}^p \hat{\mathbf{k}} \hat{\mathbf{k}}^T \mathbf{p}. \end{aligned} \quad (33)$$

Without loss of generality, we let $\hat{\mathbf{k}} = \hat{\mathbf{z}}$, $\mathbf{p} = [\sin \theta \cos \phi, \sin \theta \sin \phi, \cos \theta]$ and $d\mathbf{p} = \sin \theta d\theta d\phi$ for $\theta \in$

$[0, \pi]$, $\phi \in [0, 2\pi]$. Then, we can write

$$\begin{aligned} &(\sigma + ik \cos \theta + Dk^2) \tilde{\Psi} \\ &= -\frac{3\gamma \alpha k^2}{4\pi(k^2 + \nu^2)} \cos \theta \sin \theta [\cos \phi F_1 + \sin \phi F_2], \end{aligned} \quad (34)$$

where we have defined the integral operators of $\tilde{\Psi}$

$$\begin{aligned} F_1(\tilde{\Psi}) &= \int_0^{2\pi} \cos \phi' \int_0^\pi \sin^2 \theta' \cos \theta' \tilde{\Psi}(\theta', \phi') d\theta' d\phi' \\ F_2(\tilde{\Psi}) &= \int_0^{2\pi} \sin \phi' \int_0^\pi \sin^2 \theta' \cos \theta' \tilde{\Psi}(\theta', \phi') d\theta' d\phi' \end{aligned}$$

Eq. (33) constitutes a linear eigenvalue problem for the perturbation mode $\tilde{\Psi}$ and the growth rate σ . Applying the operator F_1 to Eq. (33), we arrive at an integral equation for σ :

$$1 = -\frac{3\gamma \alpha k^2}{4\pi(k^2 + \nu^2)} \int_0^\pi \frac{\sin^3 \theta \cos^2 \theta}{(\sigma + \lambda_0 + ik \cos \theta + Dk^2)} d\theta. \quad (35)$$

Letting $a = (\sigma + Dk^2)/ik$, we evaluate the integral and

$$1 = -\frac{3\alpha \gamma k^2}{4(k^2 + \nu^2)} \frac{1}{ik} \left[2a^3 - \frac{4a}{3} + (a^4 - a^2) \log \left(\frac{a-1}{a+1} \right) \right],$$

which we rewrite as

$$\begin{aligned} 0 &= \mathcal{F}(\sigma, k) := \\ &\frac{-4ik}{3(-\alpha\gamma)} \frac{k^2 + \nu^2}{k^2} + \left[2a^3 - \frac{4a}{3} + (a^4 - a^2) \log \left(\frac{a-1}{a+1} \right) \right]. \end{aligned} \quad (36)$$

Eq. (36) is the dispersion relation for the growth rate $\sigma(k)$ in terms of wave-numbers k .

Note that for the case of no resistance, $\nu = 0$, the dispersion relation reduces to that found by many prior studies on the collective dynamics of micro-swimmer suspensions [6, 24, 32, 33, 35, 38, 42, 43, 45, 46, 48].

B. Small-wavenumber asymptotic approximation

The dispersion relation shown in Equation (36), $\mathcal{F}(\sigma, k) = 0$ cannot be solved exactly for the growth rate $\sigma(k)$. To gain insight into the behavior of the system, we look for long-wave (small wave-number k) asymptotic solutions. For this calculation, we let $\nu = \tau k$.

We assume a power series expansion $\sigma = \sigma_0 + \sigma_1 k + \sigma_2 k^2 + \dots$ for small k . The coefficients $\sigma_0, \sigma_1, \sigma_2, \dots$, can be determined from systematically solving the equations $\mathcal{F}_0(\sigma) = 0, \mathcal{F}_1(\sigma) = 0, \mathcal{F}_2(\sigma) = 0, \dots$, where these equations arise from a power series expansion in k of the dispersion relation Eq. (36) as in $0 = \mathcal{F}(\sigma, k) = \mathcal{F}_0(\sigma) + \mathcal{F}_1(\sigma)k + \mathcal{F}_2(\sigma)k^2 + \dots$. Details of the derivation are included in [125].

We obtain two distinct asymptotic solutions, or branches, for the growth rate:

$$\sigma_{H_1}(k) = \frac{(-\alpha\gamma)}{5(1+\tau^2)} + \left[\frac{-15(1+\tau^2)}{7(-\alpha\gamma)} - D \right] k^2 + \mathcal{O}(k^4), \quad (37)$$

$$\sigma_{H_2}(k) = \left[\frac{(1+\tau^2)}{(-\alpha\gamma)} - D \right] k^2 - \frac{3\pi(1+\tau^2)^2}{4(-\alpha\gamma)^2} k^3 + \mathcal{O}(k^5). \quad (38)$$

or re-written in terms of ν

$$\sigma_{H_1}(k) = \frac{(-\alpha\gamma)k^2}{5(k^2 + \nu^2)} - \left[\frac{15(k^2 + \nu^2)}{7(-\alpha\gamma)} + Dk^2 \right] + \dots, \quad (39)$$

$$\sigma_{H_2}(k) = \left[\frac{(k^2 + \nu^2)}{(-\alpha\gamma)k^2} - Dk^2 \right] + \dots \quad (40)$$

We observe that both branches of $\sigma_H(k)$ are negative for pullers ($\alpha > 0$) for any swimmer shape γ , which means a puller suspension is stable under perturbations. Translational diffusion with rate D also has a stabilizing effect for any type of suspension, as seen in the $\mathcal{O}(k^2)$ branches of both $\sigma_{H_1}, \sigma_{H_2}$.

For pushers ($\alpha < 0$) however, $\sigma_{H_1}(k)$ can be positive for non-spherical swimmers and has its maximum of $(-\alpha\gamma)/5$ at $k = 0$ for elongated pusher swimmers $\gamma = 1$ in flows with no resistance $\tau = 0 = \nu$. The value of $\sigma_{H_1}(k = 0)$ then decreases from this maximum $(-\alpha\gamma)/5$ value for increasing ν or τ . The next term in the σ_{H_1} series shows a decrease from this maximum, with the decrease being bigger for non-zero resistance τ . For a given small wave-number k , we see that resistance lowers the value of $\sigma_{H_1}(k)$, hence resistance has an overall stabilizing effect on this branch of the growth rate for perturbations of pusher suspensions. $\sigma_{H_2}(k)$ starts at zero and is positive for small k and sufficiently small diffusion.

C. Numerical solution of the dispersion relation

We can solve numerically the dispersion relation Eq. (36), $\mathcal{F}(\sigma(k, \nu), k) = 0$ for the growth rate $\sigma(k, \nu)$ for each resistance value ν and wavenumber k by using an iterative quasi-Newton solver (e.g., Matlab's *fsolve* with a trust-region search) [125]. We start with $\nu = 0$ and then advance for small ν increments $d\nu$, and for each ν value we advance in small k increments dk starting from $k = 0$. For small k and small ν , we use as initial guess the asymptotic expansions in Eqs. (39,40). Further than that, when solving for $\sigma(k + dk, \nu + d\nu)$ we use as an initial guesses linear combinations of $\sigma(k, \nu + d\nu)$ and $\sigma(k + dk, \nu)$ and a solver tolerance of dk^2 to be able to capture the solutions.

The numerical solution for the growth rate $\sigma_H(k)$ in the case of elongated pusher swimmers ($\gamma = 1, \alpha = -1$) is shown in Fig. (3) for various resistance values ν .

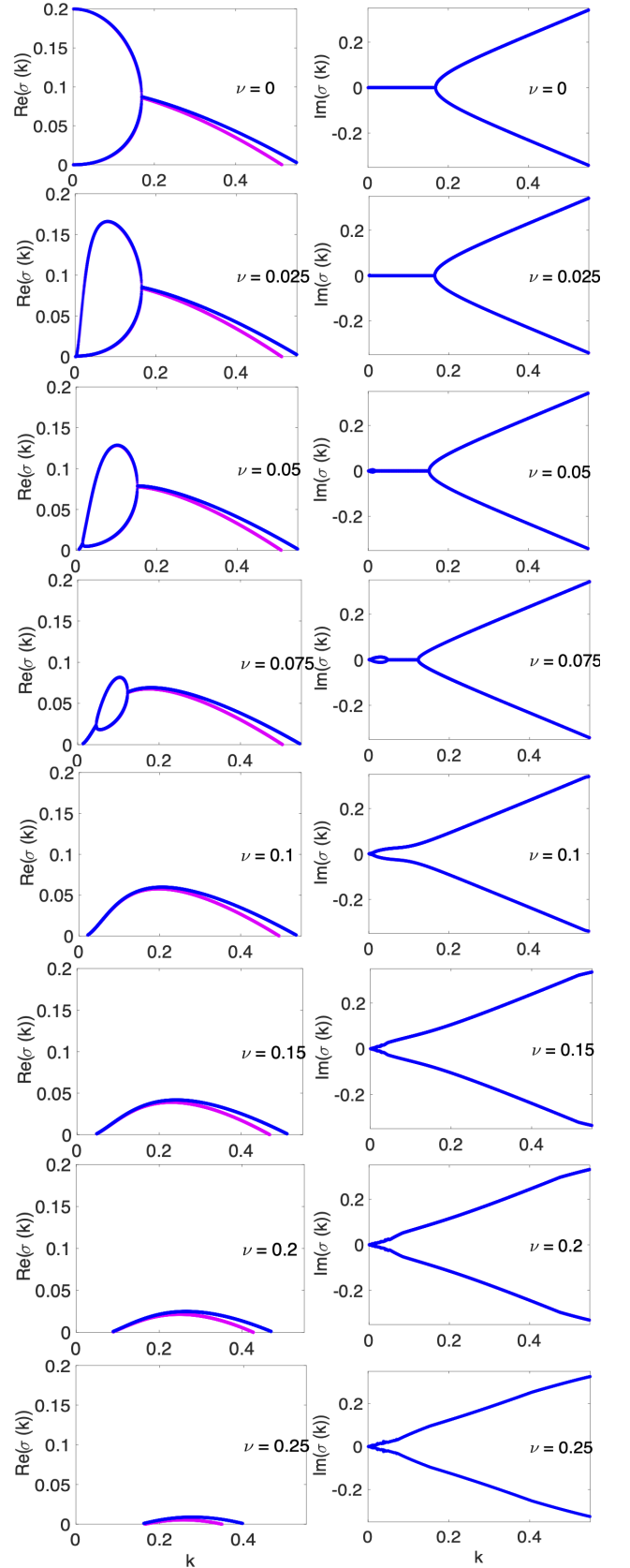


FIG. 3. Real and imaginary parts of the growth rate $\sigma_H(k)$ obtained from numerically solving Eq. (36) for various resistance parameters $\nu = 0, 0.025, \dots, 0.2$, with blue and magenta lines for $D = 0$ and $D = 0.015$ respectively.

We first discuss the results for the case of no translational diffusion $D = 0$, and start with the case of homogeneous flow i.e. $\nu = 0$. In Fig. 3 we see two branches of the growth rate, as predicted by the asymptotic analysis in Eqs. (39,40). The plots of the real and imaginary parts of $\sigma_H(k)$ are the well-known results discussed in many previous studies [6, 24, 32, 33, 35, 38, 42, 43, 45, 46, 48].

For $\nu = 0$, we see $\sigma_{H1}(k = 0) = 0.2$ and decreasing with k , and $\sigma_{H2}(k = 0) = 0$ and increasing with k , as predicted by the asymptotic analysis in Eqs. (39 - 40). There's a finite range of wavenumbers, from $k = 0$ to $k \approx 0.57$ for which $Re(\sigma_H(k)) > 0$ and $Im(\sigma_H(k)) = 0$ for both branches, hence a system corresponding to these wavenumbers would see growth of the perturbations from the uniform isotropic state. At $k_m(\nu = 0) \approx 0.18$, the real parts of the two branches of σ_H merge (subscript m is for merge), then decrease together until they cease to be positive at $k_+(\nu = 0) \approx 0.57$. The imaginary parts of σ_H branches are zero for $k < k_m(\nu = 0)$ and for $k > k_m(\nu = 0)$, they are non-zero and increase in magnitude with increasing k .

To better explain the next part, we define $k_-(\nu)$ and $k_+(\nu)$ as the bounds of the wavenumber range $k_-(\nu) < k < k_+(\nu)$ for which $Re(\sigma_H(\nu, k)) > 0$ and $Im(\sigma_H(\nu, k)) = 0$. For the homogeneous case $\nu = 0$ we have $k_-(\nu = 0) = 0$ and $k_+(\nu = 0) \approx 0.57$. We also define $k_b(\nu)$ and $k_m(\nu)$ as the bounds of the wavenumber range $k_b(\nu) < k < k_m(\nu)$ where the two branches of $Re(\sigma_H)$ separate and merge respectively. For the homogeneous case $\nu = 0$ we have $k_m(\nu = 0) \approx 0.18$, but note that a value for $k_m(\nu = 0)$ does not exist. In Fig. 4 we plot critical numbers k_-, k_b, k_m, k_+ for varying ν .

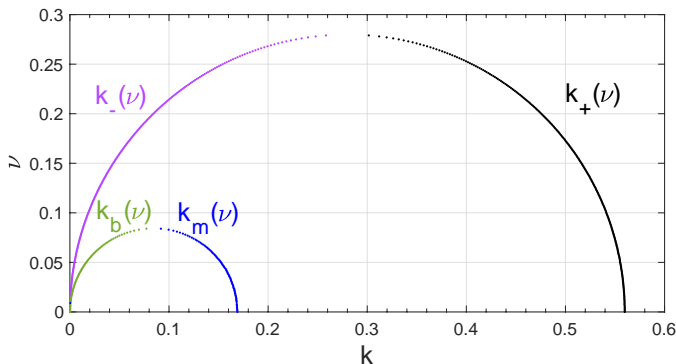


FIG. 4. Plots of the critical wavenumbers k_-, k_b, k_m, k_+ with varying resistance ν and wavenumbers k .

Next we look at the effects of non-zero but small resistance ν on the growth rate. We notice that for small $\nu \neq 0$, both growth rate branches start at zero, and they coincide $Re(\sigma_{H1}(k, \nu \neq 0)) = Re(\sigma_{H2}(k, \nu \neq 0)) = 0$ until some critical $k_b(\nu \neq 0) > 0$, which is curious as they were separate in the homogenous case $\nu = 0$. As $Im(\sigma_{H1}) = -Im(\sigma_{H2})$ for $0 < k < k_b(\nu \neq 0)$, we note that $\sigma_{H1}(k)$ and $\sigma_{H2}(k)$ are complex conjugates.

After this $k_b(\nu)$, we see $Re(\sigma_{H1})$ rise sharply, but

turn down before reaching the maximum reached by $Re(\sigma_{H1}(\nu = 0))$. For small $\nu \neq 0$, there's a range of wavenumbers $k_b(\nu) < k < k_m(\nu)$ where the two branches of $Re(\sigma_H)$ are separate but both branches of $Im(\sigma_H)(k) = 0$. In this wavenumber range $\sigma_{H1}(k)$ and $\sigma_{H2}(k)$ are both real and positive.

Beyond the merge at $k_m(\nu) < k_m(\nu = 0)$, the two $Re(\sigma_H)$ branches decrease together for increasing k until they cease to be positive for $k > k_+(\nu)$, with $k_+(\nu) < k_+(\nu = 0)$. For $k_m(\nu) < k < k_+(\nu)$ we see $Im(\sigma_{H1}) = -Im(\sigma_{H2})$, so $\sigma_{H1}(k)$ and $\sigma_{H2}(k)$ are complex conjugates again. For wavenumbers $k > k_+(\nu)$, $\sigma_{H1}(k)$ and $\sigma_{H2}(k)$ remain complex conjugates but with a negative real part.

At $\nu_c \approx 0.0806$, we have $k_b(\nu) = k_m(\nu)$ and the real parts of the two σ_H branches merge and remain merged for $\nu > \nu_c$, whereas their imaginary parts are nonzero and conjugates.

At $\nu_z \approx 0.2687$ we have $k_-(\nu) = k_+(\nu)$ and the real parts of the two σ_H branches no longer have any positive parts for any wavenumber k . Hence linear theory tells us that $\nu > \nu_z$ turns off the hydrodynamic instability for pusher suspensions for *any* wavenumber k , thus any system size.

It can be seen in Fig. (3) that translational diffusion has a stabilizing effect as it lowers both $Re(\sigma_H)$ branches by Dk^2 and does not affect $Im(\sigma_{H1})$. Puller suspensions ($\alpha > 0$) are stable, as are spherical swimmers ($\gamma = 0$), for any resistance values ν according to linear theory, hence we do not present them here. We note however that those suspensions may yet develop instabilities due to other interactions, e.g. steric or aligning [39].

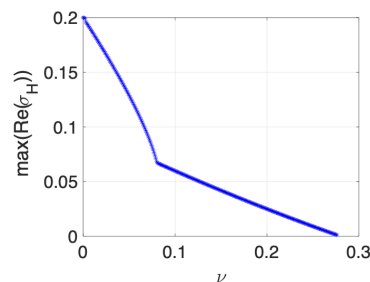


FIG. 5. Plot of $\max(Re(\sigma_H(\nu)))$ for varying resistance ν . Note the critical values $\nu_c \approx 0.0806$ and $\nu_z \approx 0.2687$.

Note from Fig. (3) and the plot of $\max(Re(\sigma_H(\nu)))$ in Fig. (5) that for any wavenumber k , if $0 < \nu_1 < \nu_2$, then $Re(\sigma_H(k, \nu = 0)) > Re(\sigma_H(k, \nu_1)) > Re(\sigma_H(k, \nu_2))$. Therefore fluctuations from the uniform isotropic state in pusher suspensions are less unstable for heterogeneous flows with increasing resistance and also less unstable than homogeneous flows. This agrees with our analysis of the system's configurational entropy.

VI. SIMULATIONS OF THE NONLINEAR SYSTEM

A. Numerical method

Linear stability analysis suggested parameters for which perturbations from the uniform isotropic state will grow for given domain sizes, but it does not tell us what the dynamics will look like. To investigate the dynamics of the motile suspensions, we perform numerical simulations of the full nonlinear system, Eqs. (23) and (24).

Since a full 3D system is computationally heavy due to three space variables and two orientation variables, we focus instead a periodic 2D system in which the particles are constrained to move and rotate in the (x, y) -plane with orientation parameterized by one angle $\theta \in [0, 2\pi)$, so that the direction is $\mathbf{p} = (\cos \theta, \sin \theta, 0)$. The domain is discretized uniformly with typically $M = 128 - 256$ points in the x and y directions and $M_\theta = 16 - 32$ points in the angle direction. We use second-order accurate finite differences to calculate the flux terms in the conservation equation. The trapezoidal rule is used to compute the integrals in orientation θ , e.g. for the active particle stresses Σ^p , swimmer density Φ .

As the computational domain is periodic, we employ spectral methods (Fast Fourier Transforms), to solve the fluid equations (24) as in Eq. (31).

Once the fluid velocity is known, we integrate the conservation Equation (23) using a second order Adams-Bashforth scheme with sufficiently small time-step to keep the calculations stable.

The initial condition is chosen to be a random perturbation around the uniform isotropic state, as also used in forerunner studies [24, 38, 46]:

$$\Psi(\mathbf{x}, \theta, 0) = \frac{1}{2\pi} \left[1 + \sum_i \epsilon_i \cos(\mathbf{k}_0 \cdot \mathbf{x} + \xi_i) P_i(\theta) \right], \quad (41)$$

where $|\epsilon_i| < 0.01$ are randomly-chosen small coefficients, ξ_i is a random phase, and $P_i(\theta)$ is a third order polynomial of $\sin(\theta)$ and $\cos(\theta)$ with random $O(1)$ coefficients.

The results presented here are for elongated pusher swimmers with $\gamma = 1$ and $\alpha = -1$. We choose a periodic square box with side $L = 25$, a size which allows for enough unstable modes according to our linear stability analysis results. Translational and rotational diffusions are included with coefficients $D = d_r = 0.01$ to ensure that the distribution function remains bounded in time.

B. The effect of the Brinkman resistance

Figs. 6 to 11 present simulations of the dynamics of an initially isotropic suspension for various values of the hydrodynamic resistance parameter, $\nu \in 0..0.25$, suggested from the linear stability analysis. The simulations consider pushers that are initially uniformly distributed and

pointing in random directions, resulting in an initial fluid flow perturbation around zero.

For ν zero or small, at short times we obtain the dynamics observed for Stokesian swimmer suspensions [24]. The fluctuations decay and the concentration field becomes smoother. The mean director and velocity fields quickly become smooth and correlated on scales on the order of the box size. At longer times the concentration field begins to develop strong fluctuations at wavelengths on the order of the box size, whereas the director and velocity fields remain correlated over large scales. The strong fluctuations are not steady in time: their magnitude stabilizes due to diffusion but their shape and position keep evolving, with dense concentration bands regions constantly merging, breaking up, and reorganizing.

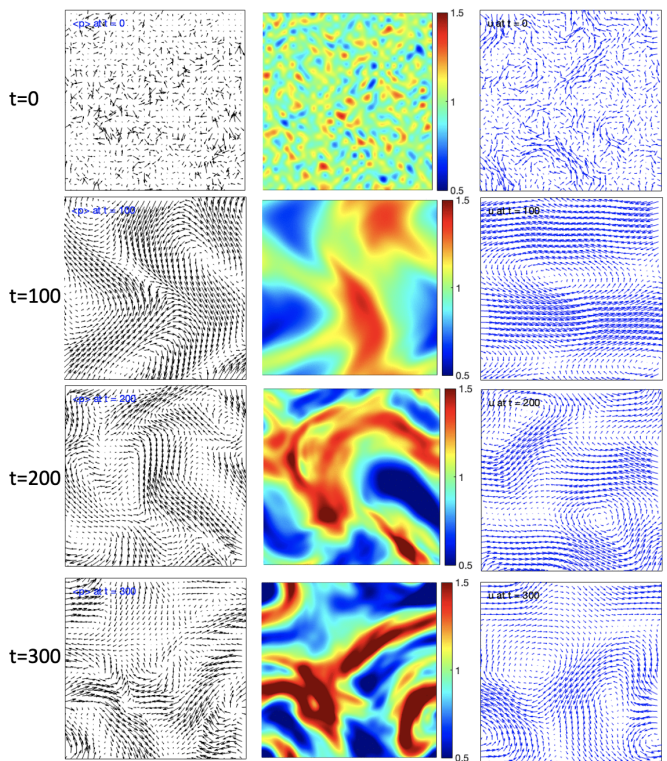


FIG. 6. The swimmer director $\langle \mathbf{p} \rangle$, concentration Φ and fluid velocity \mathbf{u} at times $t = 0, 100, 200, 300$ for $\nu = 0$.

For nonzero and increasing hydrodynamic resistance ν , e.g. $\nu = 0.1$, we notice a visible delay in the onset of the instability and a decrease in the magnitude of the concentration bands in comparison to the Stokesian case. At $\nu = 0.15$, the onset of the instability is further delayed and the concentration bands are lower, indicating a dampening effect on the fluctuations. Finally, at high hydrodynamic resistance ($\nu = 0.25$ and further), the instability is considerably suppressed, and the perturbations decay to zero. These results suggest that pushers have difficulties accumulating and moving collectively due to the higher frictional resistance.

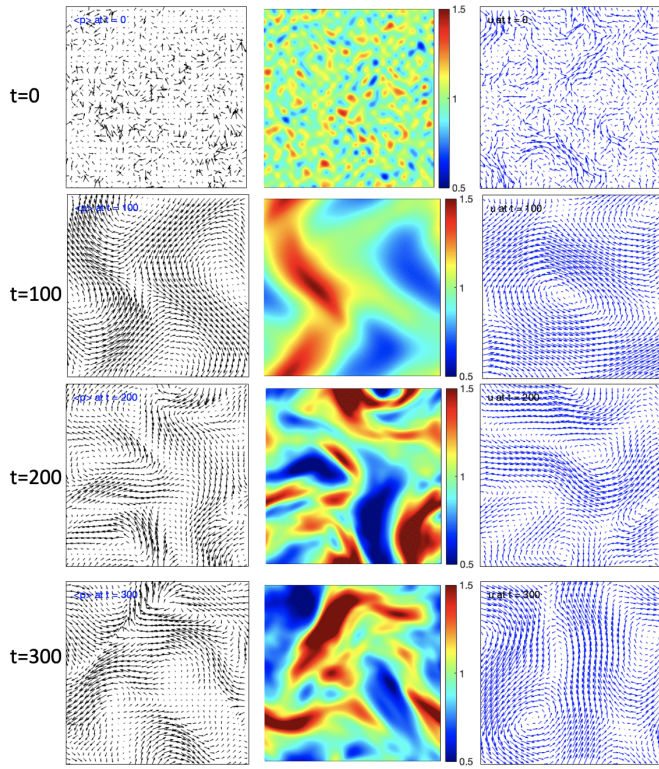


FIG. 7. The swimmer director $\langle \mathbf{p} \rangle$, concentration Φ and fluid velocity \mathbf{u} at times $t = 0, 100, 200, 300$ for $\nu = 0.05$.

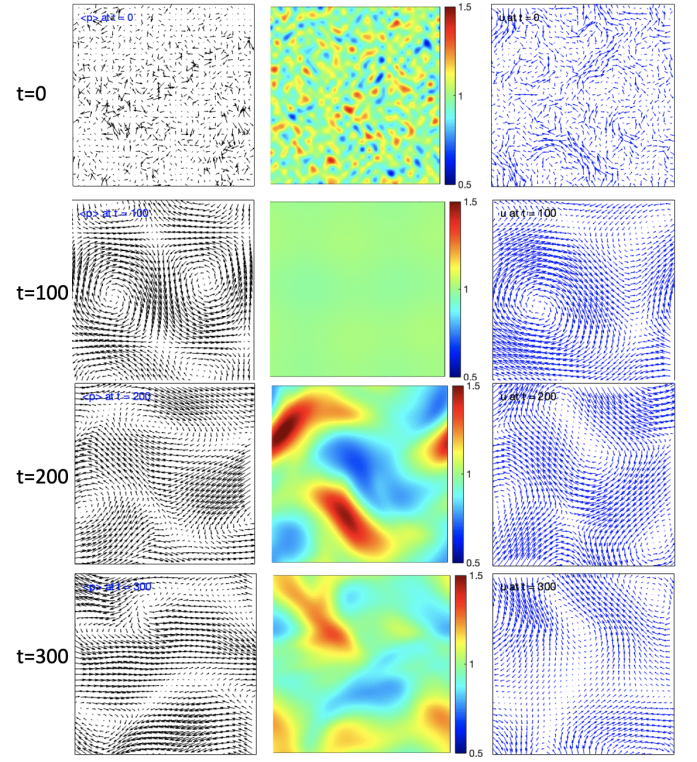


FIG. 9. The swimmer director $\langle \mathbf{p} \rangle$, concentration Φ and fluid velocity \mathbf{u} at times $t = 0, 100, 200, 300$ for $\nu = 0.15$.

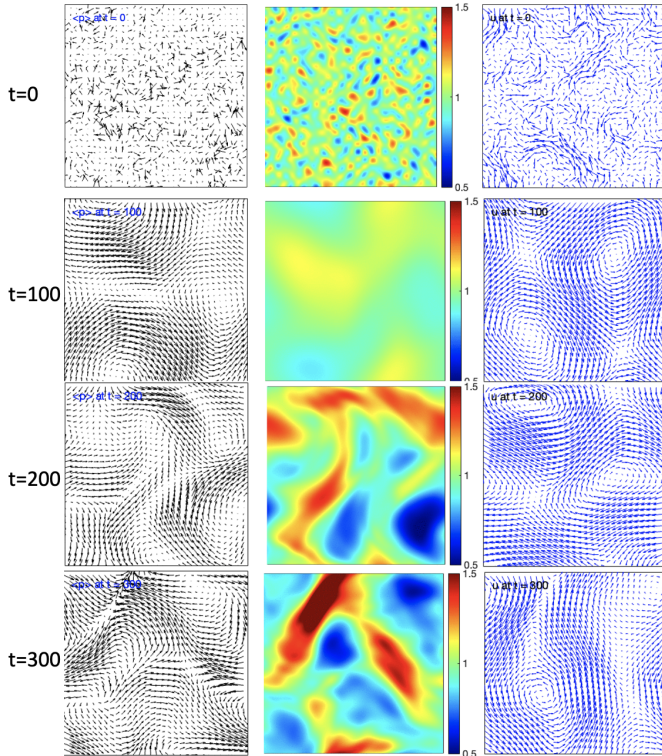


FIG. 8. The swimmer director $\langle \mathbf{p} \rangle$, concentration Φ and fluid velocity \mathbf{u} at times $t = 0, 100, 200, 300$ for $\nu = 0.1$.

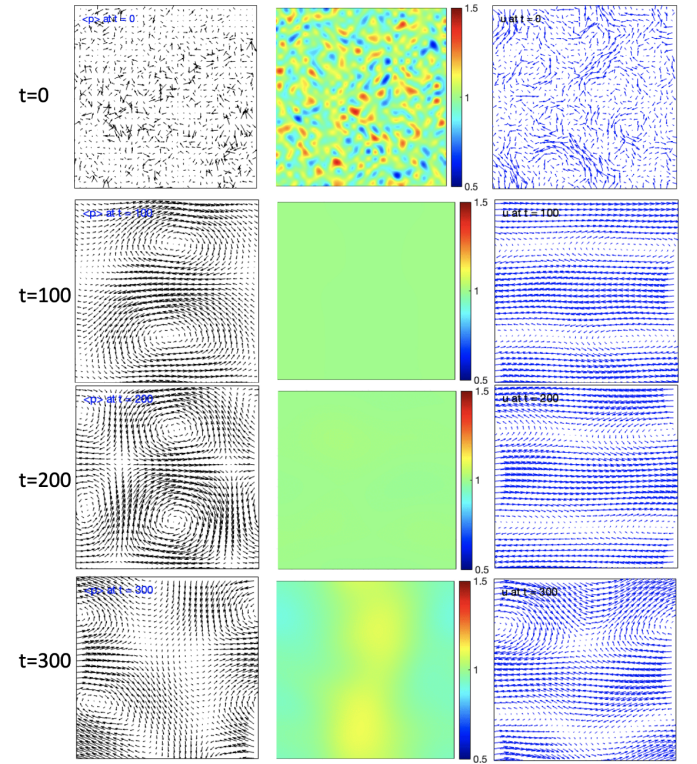


FIG. 10. The swimmer director $\langle \mathbf{p} \rangle$, concentration Φ and fluid velocity \mathbf{u} at times $t = 0, 100, 200, 300$ for $\nu = 0.2$.

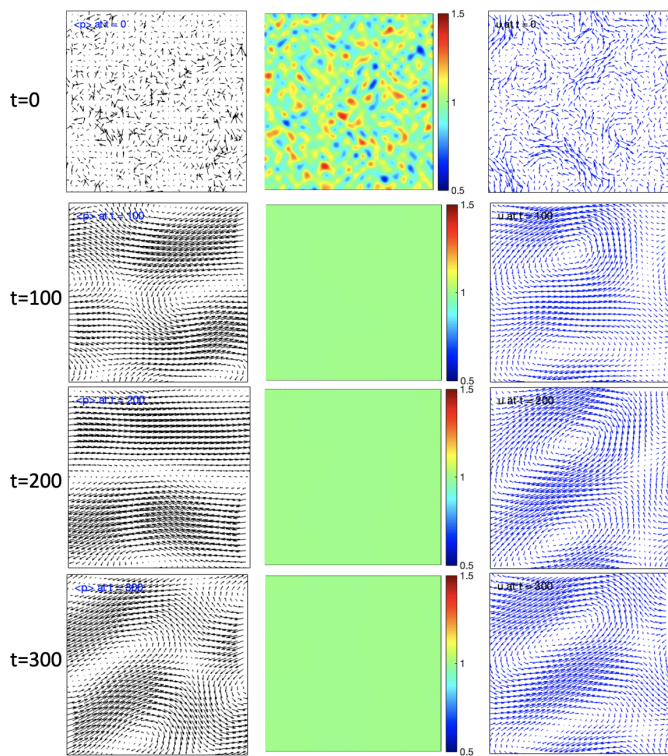


FIG. 11. The swimmer director $\langle \mathbf{p} \rangle$, concentration Φ and fluid velocity \mathbf{u} at times $t = 0, 100, 200, 300$ for $\nu = 0.25$.

The observed effects can be explained by considering the competition between the tendency of pushers to accumulate and form concentration bands and the damping effect of the fluid flow resistance. As the resistance parameter ν is increased, the frictional forces acting on the fluid and bacteria become stronger, leading to a decrease in the amplitude of the concentration bands and a delay in the onset of the instability. Moreover, at higher values of ν , the damping effect dominates over the tendency of bacteria to form concentration bands, resulting in the suppression of the hydrodynamic instability and a decrease in the collective motion of bacteria.

Lastly, recall from the linear stability analysis the critical resistance value of $\nu_z \approx 0.2687$ beyond which the hydrodynamic instability would be suppressed as $Re(\sigma_H(\nu > \nu_z)) < 0$. In Fig. 11 for $\nu = 0.25$ we saw that the initial perturbations in the suspension were fully dampened, even though $\nu = 0.25 < \nu_z$. This can be explained by the presence of other stabilizing terms such as translational and rotational diffusions, as well as the nonlinear coupling between all the terms.

C. Quantifying Brinkman resistance effects

To quantify the effect of the resistance on an initially isotropic pusher suspension, in Fig. 12 we present the evolution of three metrics in time, namely $max(\Phi)$, $mean(|\mathbf{u}|)$, and $max(|\mathbf{u}|)$, which give information about

the magnitude of the concentration bands, local fluids flows and overall averaged fluid flows. Analysis of the data presented in Fig. 12 reveals a clear trend: as the resistance is increased, the values of these metrics decrease. This trend continues until reaching a resistance value of $\nu = 0.25$, beyond which $max(\Phi)$, $mean(|\mathbf{u}|)$, and $max(|\mathbf{u}|)$ approach nearly zero values. It is evident that resistance has a dampening effect on the measured quantities, indicating its inhibitory influence.

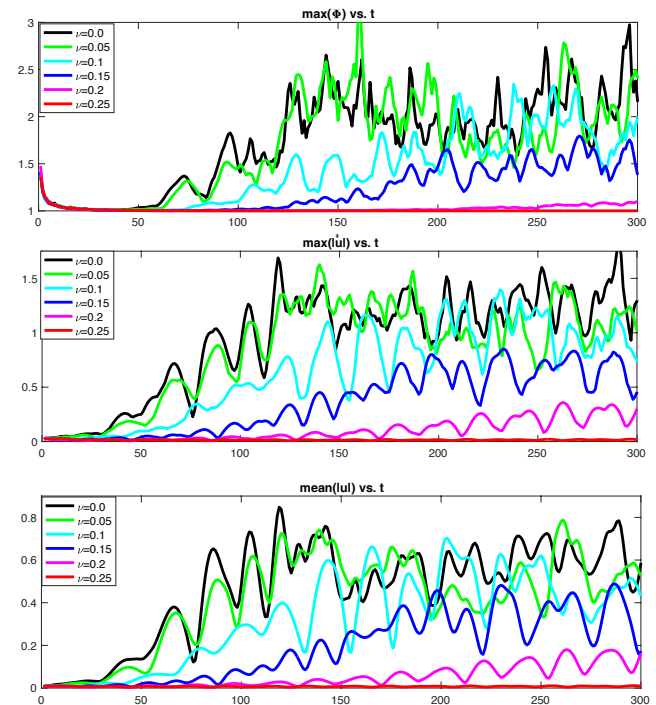


FIG. 12. Comparisons of $max(\Phi)$, $mean(|\mathbf{u}|)$, and $max(|\mathbf{u}|)$ for different ν .

As we noticed in Figs. 6 to 11 a correlation between the fluid velocity \mathbf{u} and the swimmer director $\langle \mathbf{p} \rangle$ fields, we consider the spatially-averaged contraction:

$$\langle \mathbf{u} \cdot \mathbf{n} \rangle(t) = \int d\mathbf{x} \Psi(\mathbf{x}, t) \mathbf{u}(\mathbf{x}, t) \cdot \mathbf{n}(\mathbf{x}, t), \quad (42)$$

with \mathbf{n} defined by $\Phi(\mathbf{x}, t) \mathbf{n}(\mathbf{x}, t) = \langle \mathbf{p} \rangle$. It has been known [24] that for pushers, the initially small $\langle \mathbf{u} \cdot \mathbf{n} \rangle(t)$, grows to reach a plateau, suggesting that pushers tend to align in the local disturbance flow and swim in the direction of the flow. Alignment with the flow was anticipated since the particles align in the local shear according to Jeffery's Equation (17), but here we see they on average tend to swim in the direction of the local fluid velocity. This preferred alignment and orientation result in an increase in the effective swimming velocity for pusher swimmers.

In Fig. 13 comparisons of this spatially-averaged contraction $\langle \mathbf{u} \cdot \mathbf{n} \rangle$ over time for different values of ν show that the hydrodynamic resistance decreases it, with the effect being more pronounced with increased value of ν .

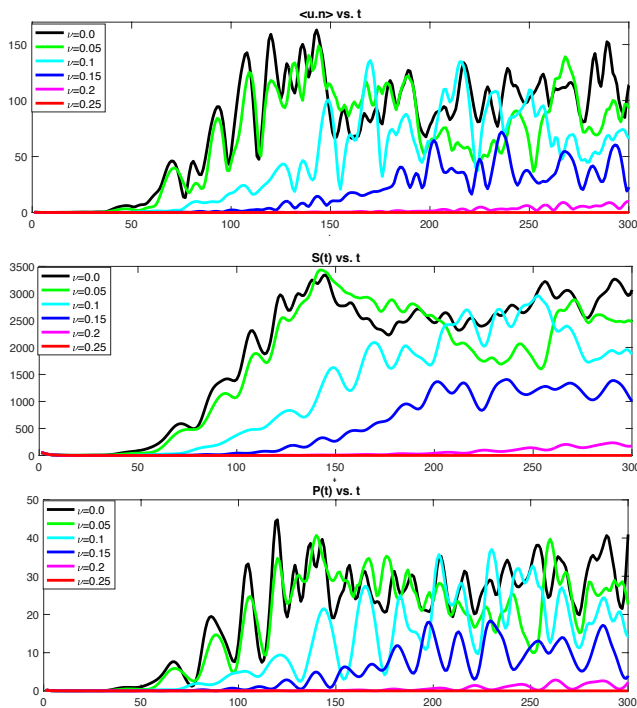


FIG. 13. Comparisons of $\langle \mathbf{u} \cdot \mathbf{n} \rangle$, entropy $\mathcal{S}(t)$ and power $P(t)$ for different ν .

Recall the system entropy $\mathcal{S}(t)$, as defined in Eq. (27), for which we obtained the exact evolution dynamics encapsulated in Eq. (30). Entropy is a thermodynamic quantity that measures the degree of disorder or randomness in a system. It is related to the availability of energy to do work and is a fundamental concept in thermodynamics, and can be used to study the behavior of fluids, such as in the context of turbulence and mixing, and is important in the study of fluid flow in complex systems [126–128].

Comparisons of the entropy $\mathcal{S}(t)$ for different values of resistance also reveal interesting trends as we can see in Fig. 13. In the absence of hydrodynamic resistance, the system experiences instability, and as a result, the entropy grows rapidly. However, as time progresses, the entropy growth rate eventually saturates, and the system enters a state of statistical equilibrium. As we introduce hydrodynamic resistance by increasing the value of ν , we observe a decrease in the system entropy. This is due to the damping effect that the resistance has on the system, which reduces the degree of disorder and randomness of the particles. When $\nu = 0.25$, the effect of hydrodynamic resistance is significant enough to prevent any instability from taking place, and the entropy decays over time.

Swimmers convert their consumed energy into motion. By examining the input power into the system generated by the swimming particles, we can gain a better understanding of how they contribute to the system dynamics.

We rewrite Eq. (29) as:

$$2 \int d\mathbf{x} \mathbf{E} : \mathbf{E} + \nu^2 \int d\mathbf{x} |\mathbf{u}|^2 = - \int d\mathbf{x} \int d\mathbf{p} (\alpha \mathbf{p} \cdot \mathbf{E} \cdot \mathbf{p}) \Psi. \quad (43)$$

The left-hand side of the equation represents the rate of viscous dissipation in the fluid, while the right-hand side represents the active input power generated by the particles. The global input power $P(t)$ is then deduced:

$$P(t) = -\alpha \int \int d\mathbf{x} d\mathbf{p} (\mathbf{p} \cdot \mathbf{E} \cdot \mathbf{p}) \Psi. \quad (44)$$

A consequence of Eq. (43) is that for pushers ($\alpha < 0$) the input power is largest when the particles are aligned with the axes of extension of the rate-of-strain tensor. This alignment occurs any particle whose orientation dynamics is governed by Jeffery’s Equation (17), thus we can expect the input power to grow in time in agreement with the existence of an instability [25].

It is clear in Fig. 13 that when there is no Brinkman resistance, the power $P(t)$ is initially small and increases with time as the hydrodynamic instability takes place, eventually reaching a plateau indicating that the system has entered a state of statistical equilibrium. When Brinkman resistance is introduced, we observe that the global input power decreases, indicating that the system requires less power to maintain the fluid flow and dynamics. The Brinkman resistance to the flow of the fluid reduces the velocity and, hence, the kinetic energy of the fluid. As the value of ν increases, the effect of the hydrodynamic resistance becomes more pronounced, and the global input power quickly decays to zero.

In both Figs. 12 and 13 we observe a consistent pattern: as the resistance parameter increases, there is a noticeable decrease in the values of all these metrics, persisting until near $\nu = 0.25$ at which the metrics exhibit a substantial reduction and approaching almost zero values. Resistance has a pronounced dampening effect on all these measured quantities, indicating its ability to hinder the onset and development of the collective swimming instabilities, and can completely suppress it if it is sufficiently large.

VII. SUMMARY AND DISCUSSION

We have used a continuum model to study the dynamics of a dilute suspension of micro-swimmers in Brinkman fluid flows. The model consists of a conservation equation for the swimmer positions and orientations, and it is coupled to the fluid flow equations in which the effect of the swimmers’ motion is represented by an active particle stress tensor, as done in many prior models [24, 31, 32, 47, 48, 104]. We include in the fluid equations a linear resistance or friction term to account for the effect of “porosity” or the inhomogeneity of the medium due to much smaller suspended particles of it.

We analyzed the stability of perturbations from the uniform isotropic state of swimmers suspensions. The exact result of the dynamics of the configurational entropy showed clearly that the Brinkman resistance has a stabilizing effect in pusher and puller suspensions alike. In pusher suspensions ($\alpha < 0$), the hydrodynamic or Brinkman resistance and the diffusion processes balance and help to drive down the increase in fluctuations resulting from the velocity gradients which in turn arose from the initial fluctuations.

The analysis of the linear stability of the isotropic suspensions lead to curious results but the same conclusion: resistance has an overall a stabilizing effect of the instability that results from the hydrodynamic interactions between the swimmers. Whereas in Stokes flow perturbation in pusher suspensions are unstable for a finite range of wave-numbers $0 \leq k \leq k_+(\nu = 0) \approx 0.57$ as a result of hydrodynamical interactions, a result meticulously studied by many colleagues [24, 25, 32, 33, 35], in Brinkman flows with $\nu \neq 0$, the pusher suspensions are unstable for a smaller range of non-zero wave-numbers $0 < k_-(\nu) < k < k_+(\nu) < k_+(\nu = 0) \approx 0.57$, and for resistance values $0 < \nu \leq \nu_z < \nu_c$. Here $\nu_z \approx 0.2687$ is the critical resistance value that linear theory suggests is the lower bound for any resistance to completely turn off the instabilities at *any* wavenumber, diffusion constants and swimmer aspect ratio in for pusher suspensions ($\alpha < 0$).

Moreover, we see some very peculiar behavior by numerically solving the dispersion relation for the growth rate that results from the linear stability analysis, Fig. 3. For Stokes flow, the shear active stresses are unstable at long wavelengths for the case of pushers (α). From the growth rate plots, low wavenumber fluctuations are expected to amplify exponentially at short times, intermediate wavenumber fluctuations amplify at a lower rate and may exhibit oscillations, whereas high wavenumber fluctuations decay while also exhibiting fluctuations. According to the linear analysis, as $Re(\sigma_H(k))$ is monotonically decreasing in Fig. 3, the lowest wavenumbers or longest wavelengths in the system, set by the box size in simulations, are expected to grow the fastest and eventually dominate the dynamics.

In Brinkman flow, the lowest wavenumber fluctuations are expected to decay at short times, perhaps with some oscillations. The intermediate wavenumber oscillations decay at a lower rate than in the case of homogenous viscous flow, and may also exhibit some oscillations. The high wavenumber fluctuations decay even faster than the Stokesian case while also exhibiting fluctuations. According to the linear analysis, the intermediate wavenumbers and wavelengths in the system, set by the box size in simulations, are expected to dominate the dynamics. Specifically, we expect the dominant wavenumber to be the one where $Re(\sigma_H(k))$ is maximized for the resistance value ν , see Figs. 3, 5.

Full nonlinear simulations of the system in two dimensions enable us to see the long-time dynamics of the

pusher suspensions and the pattern formation of the instabilities in the parameter regimes derived by the linear analysis. They confirm the prediction that Brinkman resistance has a stabilizing effect. Indeed, as expected by analysis and seen in many prior studies [24, 25], in the homogenous/ Stokes case we see the development of large-scale shear stresses, corresponding to local alignment of swimmers, and the formation of macroscopic correlated regions in the mean field director. These eventually result in strong concentration fluctuations, which are dynamically unstable and can be observed to constantly break up and merge again in quasi-periodic fashion. In the heterogeneous Brinkman flow cases, we see qualitatively similar dynamics for resistance values well below the threshold, except the onset of the instability is delayed compared to the homogeneous Stokes case, and the concentration fluctuations weaken with increased resistance values. We characterized the effect of the Brinkman resistance on the collective motion of pusher swimmers by looking at the evolution in time of several quantities such as maximum of the swimmer concentration or fluid flow, mean fluid flow, the spatially-averaged contraction, the configurational entropy, and the power input by the swimmers. These consistently show that the Brinkman resistance hinders the onset as well as the development of the collective swimming instabilities in suspensions of pushers, and can completely suppress it if sufficiently large.

These predictions have not yet been tested experimentally, though we hope that the setups of the experiments with bead-like gels [76, 80–82, 84–86], or quasi-2D disordered environments [72–74], or colloid suspensions [79], can be adapted enough to study systems where the inert micro-structure is much smaller than the swimmers and the medium can be reasonably modeled with a Brinkman approximation.

Lastly, our current model is limited to dilute non-chemotactic suspensions, but it is possible to add chemotactic interactions as in [38, 43] as well as an aligning effect to account for higher densities [39]. Moreover, the system can be adapted to study non-constant and space-dependent friction, creating the effect of soft “obstacles”, and can be used to study transport of micro-swimmers or active matter in porous media or patterned surfaces, as in [95, 96]. The combined new simulations and experiments would facilitate the development of optimized control of active suspension flows.

VIII. ACKNOWLEDGEMENTS

The authors gratefully acknowledge support from the Simons Foundation (EL) and graduate fellowships from the Kingdom of Saudi Arabia (YA). This research was supported in part by the NSF Grant No. NSF PHY-1748958 for visits at KITP. We thank T. Bhattacharjee, S. Datta, C. Hohenegger, A. Morozov, D. Saintillan, M. Shelley, and Y. Young for helpful discussions.

-
- [1] E. Lauga and T. Powers, Reports on Progress in Physics **72**, 096601 (2009).
- [2] T. J. Pedley and J. O. Kessler, Annual Review of Fluid Mechanics **24**, 313 (1992).
- [3] S. Ramaswamy, Annual Review of Condensed Matter Physics **1**, 323 (2010).
- [4] M. C. Marchetti, J. F. Joanny, S. Ramaswamy, T. B. Liverpool, J. Prost, M. Rao, and R. A. Simha, Reviews of Modern Physics **85**, 1143 (2013).
- [5] C. Bechinger, R. D. Leonardo, H. Lowen, C. Reichhardt, G. Volpe, and G. Volpe, Reviews of Modern Physics **88**, 045006 (2016).
- [6] D. Saintillan, Annual Review of Fluid Mechanics **50**, 563 (2018).
- [7] A. Martinez-Calvo, C. Trenado-Yuste, and S. Datta, arXiv , 2108.07011 (2021).
- [8] L. Cai, S. Datta, and X. Cheng, Frontiers in Physics **10**, 1005146 (2022).
- [9] S. E. Spagnolie and P. T. Underhill, Annual Review of Condensed Matter Physics **14**, 381 (2023).
- [10] W. Paxton and K. Kistler, Journal of the American Chemical Society **126**, 13424 (2004).
- [11] J. Moran and J. Posner, Phys. Today **72** **5**, 45 (2019).
- [12] M. Driscoll, B. Delmotte, M. Youssef, S. Sacanna, A. Donev, and P. Chaikin, Nature Physics **13**(4), 375 (2017).
- [13] H. Karani, G. Pradillo, and P. M. Vlahovska, Physical Review Letters **123**(20), 208002 (2019).
- [14] X.-L. Wu and A. Libchaber, Physical Review Letters **84**, 3017 (2000).
- [15] C. Dombrowski, L. Cisneros, S. Chatkaew, R. E. Goldstein, and J. O. Kessler, Physical Review Letters **93**, 098103 (2004).
- [16] M. J. Kim and K. S. Breuer, Physics of Fluids **16**, L78 (2004).
- [17] I. Tuval, L. Cisneros, C. Dombrowski, C. Wogelmueth, J.O.Kessler, and R. Goldstein, Proceedings of the National Academy of Sciences of the United States of America **102**, 2277 (2005).
- [18] L. H. Cisneros, R. Cortez, C. Dombrowski, R. E. Goldstein, and J. O. Kessler, Experiments in Fluids **43**, 737 (2007).
- [19] A. Sokolov, I. S. Aranson, J. O. Kessler, and R. E. Goldstein, Physical Review Letters **98**, 158102 (2007).
- [20] A. Sokolov, R. Goldstein, F. Feldstein, and I. Aranson, Physical Review E **80**, 031903 (2009).
- [21] H. Zhang, A. Be'er, E. Florin, and H. Swinney, Proceedings of the National Academy of Sciences of the United States of America **107**, 10731 (2010).
- [22] G. Mino, T. Mallouk, T. Darnige, M. Hoyos, J. Dauchet, J. Dunstan, R. Soto, Y. Wang, A. Rousselet, and E. Clement, Physical Review Letters **106**, 061916 (2011).
- [23] D. Saintillan and M. J. Shelley, Physical Review Letters **99**, 058102 (2007).
- [24] D. Saintillan and M. J. Shelley, Physical Review Letters **100**, 178103 (2008).
- [25] D. Saintillan and M. J. Shelley, Physics of Fluids **20**, 123304 (2008).
- [26] E. Lushi and C. Peskin, Computers and structures **122**, 4 (2013).
- [27] E. Lushi, H. Wioland, and R. Goldstein, Proceedings of the National Academy of Sciences of the United States of America **111**, 9734 (2014).
- [28] H. Wioland, E. Lushi, and R. E. Goldstein, New Journal of Physics **18**, 075002 (2016).
- [29] N. Hill and T. Pedley, Fluid Dynamics Research **37**, 1 (2005).
- [30] I. S. Aranson, A. Sokolov, J. O. Kessler, and R. E. Goldstein, Physical Review E **75**, 040901 (2007).
- [31] A. Baskaran and M. C. Marchetti, Proceedings of the National Academy of Sciences of the United States of America **106**, 15567 (2009).
- [32] G. Subramanian and D. L. Koch, Journal of Fluid Mechanics **632**, 359 (2009).
- [33] C. Hohenegger and M. J. Shelley, Physical Review E **81**, 046311 (2010).
- [34] T. Pedley, Journal of Fluid Mechanics **647**, 335 (2010).
- [35] G. Subramanian and D. L. Koch, Annual Review of Fluid Mechanics **43**, 637 (2011).
- [36] B. Ezhilan, A. A. Pahlavan, and D. Saintillan, Physics of Fluids **24**, 091701 (2012).
- [37] T. V. Kasyap and D. L. Koch, Physical Review Letters **108**, 038101 (2012).
- [38] E. Lushi, R. E. Goldstein, and M. J. Shelley, Physical Review E **86**, 040902 (2012).
- [39] B. Ezhilan, M. J. Shelley, and D. Saintillan, Physics of Fluids **25**, 070607 (2013).
- [40] J. Dunkel, S. Heidenreich, K. Drescher, H. H. Wensink, M. Bär, and R. E. Goldstein, Physical Review Letters **110**, 228102 (2013).
- [41] T. V. Kasyap and D. L. Koch, Journal of Fluid Mechanics **741**, 619 (2014).
- [42] D. Krishnamurthy and G. Subramanian, Journal of Fluid Mechanics **781**, 422 (2015).
- [43] E. Lushi, Physical Review E **94**, 022414 (2016).
- [44] M. B. Amar, Scientific Reports **6**, 21269 (2016).
- [45] J. Stenhammar, C. Nardini, R. W. Nash, D. Marenduzzo, and A. Morozov, Physical Review Letters **119**, 028005 (2017).
- [46] E. Lushi, R. E. Goldstein, and M. J. Shelley, Physical Review E **98**, 052411 (2018).
- [47] C. Miles, A. Evans, M. Shelley, and S. Spagnolie, Physical Review Letters **122**, 098002 (2019).
- [48] V. Škultéty, C. Nardini, J. Stenhammar, D. Marenduzzo, and A. Morozov, Physical Review X **10**, 031059 (2020).
- [49] N. Murugan and A. Roy, Journal of Fluid Mechanics **934**, A21 (2022).
- [50] A. Villa-Torrealba, S. Navia, and R. Soto, Physical Review E **107**, 034605 (2023).
- [51] R. Dillon, L. Fauci, and D. Gaver, Journal of Theoretical Biology **177**, 325 (1995).
- [52] M. Hopkins and L. Fauci, Journal of Fluid Mechanics **455**, 149 (2002).
- [53] T. Ishikawa, M. P. Simmonds, and T. J. Pedley, Journal of Fluid Mechanics **568**, 119 (2006).
- [54] J. Hernandez-Ortiz, P. Underhill, and M. Graham, Journal of Physics: Condensed Matter **21**, 204107 (2007).
- [55] T. Ishikawa, T. J. Pedley, and T. Yamaguchi, Journal of Theoretical Biology **249**, 296 (2007).

- [56] T. Ishikawa and T. J. Pedley, *Journal of Fluid Mechanics* **588**, 437 (2007).
- [57] T. Ishikawa and T. J. Pedley, *Journal of Fluid Mechanics* **588**, 399 (2007).
- [58] T. Ishikawa and T. J. Pedley, *Physical Review Letters* **100**, 088103 (2008).
- [59] P. T. Underhill, J. P. Hernandez-Ortiz, and M. D. Graham, *Physical Review Letters* **100**, 248101 (2008).
- [60] J. Hernandez-Ortiz, C. Stoltz, and M. Graham, *Journal of Physics* **21**, 204107 (2009).
- [61] D. Saintillan and M. Shelley, *Journal of the Royal Society Interface* (2011).
- [62] J. Elgeti, R. G. Winkler, and G. Gompper, *Reports on Progress in Physics* **78**, 056601 (2015).
- [63] A. Zottl and H. Stark, *Journal of Physics: Condensed Matter* (2016).
- [64] F. Rojas-Pérez, B. Delmotte, and S. Michelin, *Journal of Fluid Mechanics* **A22**, 919 (2021).
- [65] T. Traverso and S. Michelin, *Journal of Fluid Mechanics* **A21**, 943 (2022).
- [66] S. Michelin, *Annual Review of Fluid Mechanics* **55**, 77 (2023).
- [67] G. Li, E. Lauga, and A. Ardekani, *Journal of Non-Newtonian Fluid Mechanics* **297**, 104655 (2021).
- [68] R. D. Leonardo, L. Angelani, D. Dell'Arciprete, G. Ruocco, V. Iebba, S. Schippa, M. P. Conte, F. Mecarini, F. D. Angelis, and E. D. Fabrizio, *Proceedings of the National Academy of Sciences of the United States of America* **107**, 9541 (2010).
- [69] A. Sokolov, M. M. Apodaca, B. A. Grzybowski, and I. S. Aranson, *Proceedings of the National Academy of Sciences of the United States of America* **107**, 969 (2010).
- [70] H. Wioland, F. Woodhouse, J. Dunkel, J. Kessler, and R. Goldstein, *Physical Review Letters* **110**, 268102 (2013).
- [71] W. F. Paxton, K. C. Kistler, C. C. Olmeda, A. Sen, S. K. S. Angelo, Y. Cao, T. E. Mallouk, P. E. Lammer, and V. H. Crespi, *Nature Communications* **9**, 4486 (2018).
- [72] S. Makarchuk, V. Braz, N. Araujo, L. Ciric, and G. Volpe, *Nature Communications* **10**, 4110 (2019).
- [73] A. Dehkharghani, N. Waisbord, J. Dunkel, and J. S. Guasto, *Proceedings of the National Academy of Sciences* **116**, 11119 (2019).
- [74] A. Dehkharghani, N. Waisbord, and J. S. Guasto, *Communications Physics* **6**, 18 (2023).
- [75] G. Volpe, I. Buttinoni, D. Vogt, J.-H. Kummerer, and C. Bechinger, *Soft Matter* **7**, 8810 (2011).
- [76] T. Majmudar, E. Keaveny, J. Zhang, and M. J. Shelley, *Journal of the Royal Society Interface* **9**, 1809 (2012).
- [77] M. Contino, E. Lushi, I. Tuval, V. Kantsler, and M. Polin, *Physical Review Letters* **115**, 258102 (2015).
- [78] O. Sipoș, K. Nagy, R. D. Leonardo, and P. Galajda, *Physical Review Letters* **114**, 258104 (2015).
- [79] S. Kamdar, S. Shin, P. Leishangthem, L. Francis, X. Xu, and X. Cheng, *Nature* **603**, 819 (2022).
- [80] T. Bhattacharjee and S. S. Datta, *Nature Communications* **1**, 2 (2019).
- [81] T. Bhattacharjee and S. S. Datta, *Soft Matter* **15**, 9920 (2019).
- [82] D. Amchin, J. Ott, T. Bhattacharjee, and S. Datta, *PLoS Computational Biology* **18**, e1010063 (2022).
- [83] T. Bhattacharjee, D. Amchin, J. Ott, F. Kratz, and S. Datta, *Biophysical Journal* **120**, 3483 (2021).
- [84] T. Bhattacharjee, D. B. Amchin, R. A. J. A. Ott, and S. Datta, *eLife* **11**, e71226 (2022).
- [85] A. Martinez-Calvo, T. Bhattacharjee, R. Bay, H. Luu, A. Hancock, N. Wingreen, and S. Datta, *Proceedings of the National Academy of Sciences U.S.A.* **119** (43), e2208019119 (2022).
- [86] J. Moore-Ott, S. Chiu, D. Amchin, T. Bhattacharjee, and S. Datta, *Elife* **11**, e76380 (2022).
- [87] R. Alert, J. Casademunt, and J. Joanny, *Annual Review of Condensed Matter Physics* **13**, 143 (2022).
- [88] C. Datt, L. Zhu, G. Elfring, and O. Pak, *Journal of Fluid Mechanics* **784**, R1 (2015).
- [89] C. Datt, G. Natale, S. Hatzikiriakos, and G. Elfring, *Journal of Fluid Mechanics* **823**, 675 (2017).
- [90] Z. Kos and M. Ravnik, *Fluids* **3**, 1 (2018).
- [91] Y. Bozorgi and P. T. Underhill, *Journal of Rheology* **57**, 511 (2013).
- [92] Y. Bozorgi and P. T. Underhill, *Journal of Non-Newtonian Fluid Mechanics* **214**, 69 (2014).
- [93] G. Li and A. Ardekani, *Physical Review Letters* **117**(11), 118001 (2016).
- [94] N. Desai and A. Ardekani, *Soft Matter* **13**, 6033 (2017).
- [95] R. L. Stoop, N. Waisbord, V. Kantsler, V. Heinonen, J. Guasto, and J. Dunkel, *Journal of Non-Newtonian Fluid Mechanics* **268**, 66 (2019).
- [96] K. Thijssen, D. Khaladj, Aghvami, S. Ali, M. Gharbi, S. Fraden, J. Yeomans, L. Hirst, and T. Shendruk, *Proceedings of the National Academy of Sciences of the United States of America* **2102.10184**, 13 (2021).
- [97] M. Kumar, J. S. Guasto, and A. M. Ardekani, *Journal of Rheology* **66**, 375 (2022).
- [98] K. Leiderman and S. D. Olson, *Physics of Fluids* **28**, 1 (2016).
- [99] H. Nganguia and O. S. Pak, *Journal of Fluid Mechanics* **855**, 554 (2018).
- [100] H. Nguyen, K. Leiderman, and S. Olson, *Journal of Fluid Mechanics* **864**, 1088 (2019).
- [101] H. Nguyen, S. Olson, and K. Leiderman, *Journal of Engineering Mathematics* **114**, 19 (2019).
- [102] H. Nganguia, L. Zhu, D. Palaniappan, and O. S. Pak, *Physical Review E* **101**, 063105 (2020).
- [103] C. Jeznach and S. D. Olson, *Fluids* **5** (2020).
- [104] R. A. Simha and S. Ramaswamy, *Physica A* **306**, 262 (2002).
- [105] S. Jung, *Physics of Fluids* **22**, 1 (2010).
- [106] N. Charon, E. Greenberg, M. Koopman, and R. Limberger, *Research in Microbiology* **143**, 597 (1992).
- [107] R. Cortez, B. Cummins, K. Leiderman, and D. Varela, *Journal of Computational Physics* **229**, 7609 (2010).
- [108] H. Brinkman, *Applied Scientific Research Section A* **1**, 27 (1947).
- [109] H. C. Brinkman, *Appl. Sci. Res.* **1**, 27 (1949).
- [110] L. Durlafsky and J. Brady, *Physics of Fluids* **30**, 3329 (1987).
- [111] A. Daddi-Moussa-Ider, Y. Hosaka, A. Vilfan, and R. Golestanian, *arXiv preprint*, 2305.07669 (2023).
- [112] H. Nguyen, S. Olson, and K. Leiderman, *Computers and Fluids* **133**, 55 (2016).
- [113] C. Hohenegger and M. J. Shelley, *Oxford University Press, New York* **92**, 66 (2011).
- [114] G. Batchelor, *Journal of Fluid Mechanics* **44**, 419 (1970).
- [115] J. Keller and S. Rubinow, *Journal of Fluid Mechanics* **75**, 705–714 (1976).

- [116] R. Johnson, *Journal of Fluid Mechanics* **99**, 411–431 (1980).
- [117] G. K. Batchelor, *Journal of Fluid Mechanics* **41**, 545 (1970).
- [118] G. K. Batchelor, *Journal of Fluid Mechanics* **83**, 97 (1977).
- [119] M. Doi and S. Edwards, *The Theory of Polymer Dynamics* (Oxford University Press, New York, 1986).
- [120] R. Larson, *The Structure and Rheology of Complex Fluids* (Oxford University Press, New York, 1995).
- [121] G. B. Jeffrey, *Proceedings of the Royal Society* **102**, 161 (1922).
- [122] K. Chen, R. Ford, and P. Cummings, *Journal of Mathematical Biology* **47**, 518 (2003).
- [123] S. Childress, *The Journal of Chemical Physics* **56**, 2527 (1972).
- [124] J. M. Yeomans, D. Pushkin, and H. Shum, *The European Physical Journal Special Topics* **223**, 1771–1785 (2014).
- [125] Y. Almoteri, *Bacterial motion and spread in porous environments*, Ph.D. thesis, New Jersey Institute of Technology (2023).
- [126] P. Kundu and I. Cohen, *Fluid mechanics*, 6th ed. (Academic Press, Massachusetts, 2016).
- [127] A. Bejan, *Advanced engineering thermodynamics*, 4th ed. (Wiley, New York, 2013).
- [128] H. Callen, *Thermodynamics and an introduction to thermostatistics*, 2nd ed. (New York, Wiley, 1985).